




Influence of Er^{3+} ions on the physical, structural, optical, and thermal properties of $\text{ZnO-Li}_2\text{O-P}_2\text{O}_5$ glasses

M. Shwetha¹ · B. Eraiah¹ Received: 16 November 2018 / Accepted: 7 February 2019 / Published online: 2 March 2019
© Springer-Verlag GmbH Germany, part of Springer Nature 2019

Abstract

Er^{3+} doped zinc lithium phosphate glass samples were synthesized by the very simple melt quenching method. The obtained X-ray diffraction patterns specify that the prepared glass samples exhibit glassy nature. The physical properties like packing density, molar volume, density, oxygen packing density, interionic distance, field strength, rare earth ion concentration, and polaron radius were calculated using appropriate formulae. DTA curve was analysed to evaluate the crystallization temperature, melting temperature, and glass transition temperature and hence study the thermal properties. Fourier transform infrared spectrum was recorded to examine the functional groups in the glass and study the structural characteristics of the glass. It showed the presence of symmetrical and asymmetrical stretching vibration modes of P–O–P linkages, bending modes of P–O in PO_4 , bending and stretching vibrations of OH groups and P–O–H water absorbance in the glasses. The absorption spectra of the prepared glasses in the UV–visible region (wavelength 200–1100 nm) were taken to study the optical properties of the glasses. The Urbach energy and optical energy bandgap values are determined using Davis–Mott method. The refractive index of all the prepared glass samples is also measured and these values are used to determine the corresponding molar refraction, the molecular polarizability of oxide ions, dielectric constant, reflection loss, metallization criterion, electronic polarizability of the oxide ions, interaction parameter, electronegativity, optical basicity, and electric susceptibility of all the glass samples using appropriate formulae.

1 Introduction

Glasses with lanthanide ions are nowadays grabbing utmost attention attributable to their widespread impending applications in development of laser hosts, optical sensors, optical displays, optical fibres, optical readers, multicolour phosphors, photodiodes, etc. [1–6], because these ions exhibit substantial features like extensive lifetime, various emission and absorption bands from UV to IR region and various excited energy levels. Higher transparency and also easy method of preparing glasses with different compositions make oxide glasses especially phosphate-based glasses more advantageous and suitable for hosting rare earth ions [7–10]. Phosphate glasses also possess distinctive properties like low glass transition and melting temperature, high UV and IR transitions, lesser dispersion, good solubility of lanthanide ions [11–15]. In this glass matrix, ZnO acts as a network

former in addition to being a network modifier depending on the chemical composition and Li_2O acts a glass modifier [16–18]. Zinc Oxide is generally used in phosphate glasses due to its non-hygroscopic and non-toxic nature which helps to reduce the tendency of the phosphate-based glasses to absorb moisture from the air [19]. The presence of Li_2O aids in decreasing the hygroscopic nature and also help in increasing the chemical resistance and polarization of the glasses [20, 21]. Out of all the known rare earth ions which generally help in optically exciting the glasses, Er^{3+} ions are extremely helpful because these ions have high emission cross-section, broad bands of emission, longer lifetime, and high quantum efficiency [22, 23] which plays a very important role in photonics like telecommunication, designing optical devices like 3d displays, optical readers, etc. [24–26].

In this paper, the thermal properties, optical properties, structural properties and physical parameters of Er^{3+} doped zinc lithium phosphate glasses have been examined and reported.

✉ B. Eraiah
eraiah@rediffmail.com

¹ Department of Physics, Bangalore University, Bangalore, Karnataka 560056, India

2 Experimental details

By melt quenching, Er^{3+} doped zinc lithium phosphate glasses with glass formula, $x\text{mol}\% \text{Er}_2\text{O}_3 - 40\text{mol}\% \text{P}_2\text{O}_5 - 45\text{mol}\% \text{ZnO} - (15-x)\text{mol}\% \text{Li}_2\text{O}$ (where $x=0, 0.1, 0.3, 0.5, 1, 1.5$ and $2\text{mol}\%$) are prepared. Analar grade chemicals (Er_2O_3 , $\text{LiOH}\cdot\text{H}_2\text{O}$, ZnO , and $\text{NH}_4\text{H}_2\text{PO}_4$) were weighed (about 8 g per batch) and mixed carefully by grinding in an agate mortar. The blend was then transferred to porcelain crucibles. The crucibles were marked accordingly and placed inside a muffle furnace which was set to 1150°C for 1 h to get a homogenous liquid. The liquid was then immediately quenched using pre-heated brass moulds and brass blocks. The obtained glass samples were transparent, pink in colour and they were annealed (300°C for 2 h) to achieve structural and thermal sturdiness. The glasses obtained of suitable sizes were polished, named as PZLE0, PZLE01, PZLE03, PZLE05, PZLE10, PZLE15 and PZLE20 for varying concentrations of Er_2O_3 i.e., for $x=0, 0.1, 0.3, 0.5, 1, 1.5$ and $2\text{mol}\%$, respectively, and were used for studying various properties. X-ray diffraction spectra were taken from RIGAKU, ULTIMA IV X-ray diffractometer operated at $40\text{ kV}/30\text{ mA}$, using $\text{Cu K}\alpha$ radiation of wavelength $\lambda=1.5406\text{ \AA}$. Archimedes procedure was followed at room temperature to estimate the densities of the glasses. Fourier transform infra-red spectra were obtained following KBR pellet technique in $400\text{--}4000\text{ cm}^{-1}$ spectral range and resolution of 4 cm^{-1} using Thermo Nicolet, Avatar 370 FTIR spectrometer. DTA curve was taken from Simultaneous Thermal Analyser, PerkinElmer STA 6000 in nitrogen atmosphere from 20 to 900°C at 10°C per minute heating rate. Refractive index values were measured from digital Abbe refractometer ATAGO at 589.3 nm wavelength. Optical absorption spectra for all the glasses at room temperature from 200 to 1100 nm were recorded from Shimadzu UV-1800 Spectrophotometer operated at $220\text{--}240\text{ V}$.

3 Results and discussion

3.1 X-ray diffraction (XRD) analysis

Figure 1 shows the XRD pattern obtained for the prepared glass sample with $0.5\text{ mol}\% \text{Er}_2\text{O}_3$. A broad hump instead of any sharp peaks is observed for all the glasses between 15° and 35° , which indicates the non-crystalline nature of the glasses prepared.

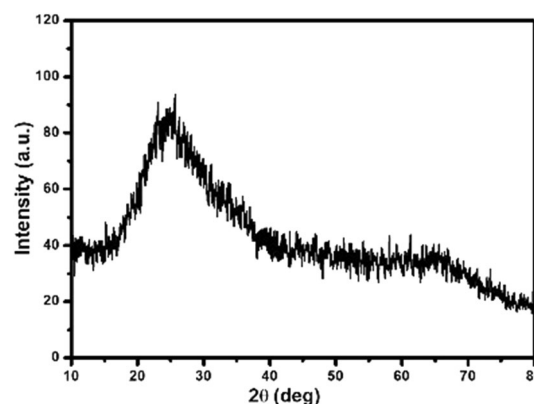


Fig. 1 XRD pattern of PZLE05 glass sample

3.2 Physical properties

3.2.1 Density, molar volume, and average phosphorus–phosphorus separation

Density was calculated from the Archimedes technique by measuring the weight of the glass in air (w_a), its weight when submerged in toluene (w_t) and applying to the well-known formula,

$$\frac{\rho}{\rho_t} = \frac{w_a}{(w_a - w_t)} \quad (1)$$

(where ρ_t , density of toluene $= 0.866\text{ g/cm}^3$). The equation which relates molar volume, molecular weight, and density of the glass sample given by,

$$V_m = M/\rho, \quad (2)$$

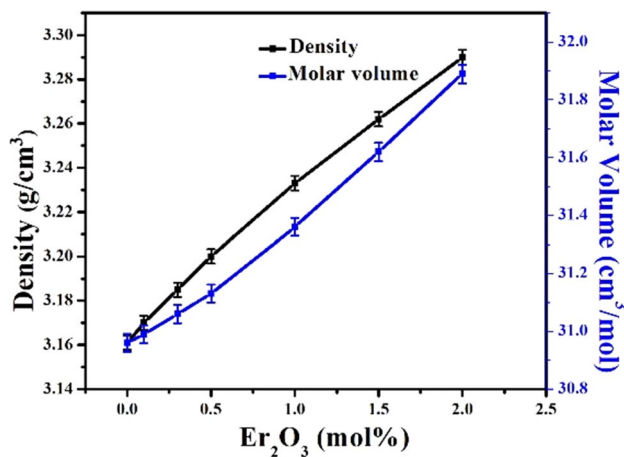
was used to calculate the molar volume. Calculated molar volume and density of all the glass samples are listed in Table 1. Density and molar volume of the glass samples are found to be increasing from 3.161 to 3.290 g/cm^3 and 30.96 to $31.89\text{ cm}^3/\text{mol}$, respectively, as a result of the network modification in the structure of glass caused by the incorporation of higher molecular weight compound erbium oxide (333 g/mol , which is heavier than all the other compounds present in the matrix) and also may be due to the increasing number of the non-bridging oxygen on increasing the quantity of Er_2O_3 . The correlation of the molar volume, V_m and density, ρ of the glasses with Er_2O_3 are shown in Fig. 2.

The influence of Er_2O_3 content on the glass system can be analysed by calculating the average phosphorus–phosphorus separation. It can be calculated using [27]

$$\langle d_{\text{P-P}} \rangle = \left(\frac{V_m}{2N_A(1 - X_P)} \right)^{1/3}. \quad (3)$$

Table 1 Density, ρ (g/cm³), molar volume, V_m (cm³/mol), Er³⁺ ions concentration, N_{RE} (ions/cm³), polaron radius, r_{pn} (Å), interionic distance, d (Å), field strength, F (cm⁻²), packing density (V_p), averagephosphorus–phosphorus distance, d_{p-p} (g.atom/l), oxygen packing density (OPD), number of bonds per unit volume, n_b (m⁻³) and coordination number (m)

x (mol%)	ρ	V_m	N_{RE} $\times 10^{21}$	r_{pn}	d	F $\times 10^{16}$	V_p	$\langle d_{p-p} \rangle$ $\times 10^{-2}$	OPD	n_b $\times 10^{29}$	m
	± 0.001	± 0.01	± 0.001	± 0.01	± 0.01	± 0.001	± 0.0001	± 0.01	± 0.01	± 0.001	± 0.001
0	3.161	30.96	—	—	—	—	0.6032	349.91	83.97	0.778	4.000
0.1	3.170	30.99	1.943	3.22	8.01	2.877	0.6030	350.02	83.96	0.777	4.002
0.3	3.185	31.06	5.815	2.24	5.56	5.973	0.6029	350.28	83.90	0.776	4.006
0.5	3.2	31.13	9.669	1.89	4.69	8.389	0.6028	350.55	83.84	0.775	4.010
1.0	3.233	31.36	19.199	1.50	3.73	13.244	0.6013	351.41	83.54	0.771	4.020
1.5	3.262	31.62	28.560	1.31	3.27	17.269	0.5992	352.38	83.17	0.767	4.030
2.0	3.290	31.89	37.762	1.20	2.98	20.791	0.5970	353.38	82.78	0.762	4.040

**Fig. 2** Variation of density and molar volume with Er₂O₃ concentration

It is found that d_{p-p} is increasing from 349.91 to 353.38 g atom/l with increasing concentration of Er₂O₃.

3.2.2 Packing density and oxygen packing density

Packing density, V_d gives the measurement of rigidity of the oxide system [28] which may be determined by the formula,

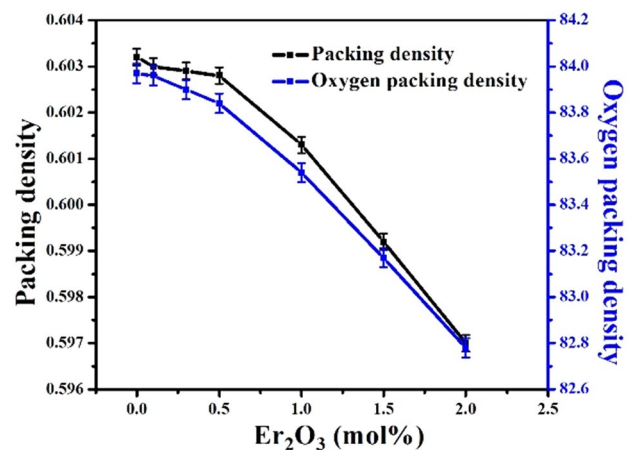
$$V_d = \frac{1}{V_m} \sum V_i X_i, \quad (4)$$

where V_i and X_i represent the packing factor and mole fraction of the composition, respectively.

Packing factor [29] of any oxide D_xO_y having D and O ions with ionic radii r_D and r_O may be estimated by:

$$V_i = \frac{4\pi N_A}{3} (Xr_M^3 + Yr_O^3). \quad (5)$$

V_i of Li₂O, ZnO and P₂O₅ are available in the literature [29], for Er₂O₃ it is 27.91 cm³/mol, calculated using Eq. 5.

**Fig. 3** Variation of packing density and OPD with Er₂O₃ concentration

It is found that the packing density decreases from 0.61 to 0.32 with increasing concentration of Er₂O₃ which is leading to the increased molar volume values indicating the rigidity of the glasses.

Oxygen packing density which defines the organisation of oxygen atoms in the glasses [30] was calculated from the formula,

$$OPD = \frac{1000 \times O}{V_m}, \quad (6)$$

where O refers to the number of oxygen atoms in the glass network.

The behaviour of oxygen packing density and packing density with Er₂O₃ composition is presented in Fig. 3. It is observed that there is a deviation occurred at 1 mol% Er₂O₃ concentration which is due to the generation of more number of non-bridging oxygen and the changes that have occurred in bonds.

Table 2 Melting temperature (T_m), crystallization temperature (T_p), onset crystallization temperature (T_c), glass transition temperature (T_g), thermal stability (T_s), glass forming ability (K), reduced glass transition temperature (T_{rg}) and thermal stability parameter (S)

x (mol%)	T_m (°C) ± 1	T_p (°C) ± 1	T_c (°C) ± 1	T_g (°C) ± 1	T_s (°C) ± 1	K (°C) ± 0.05	T_{rg} (°C) ± 0.01	S (°C) ± 0.05
0	658	540	488	356	132	0.77	0.54	19.28
0.1	660	545	494	361	133	0.80	0.58	18.78
0.3	662	550	503	364	139	0.87	0.56	18.85
0.5	681	558	513	369	144	0.85	0.55	17.56
1	698	569	520	370	150	0.84	0.52	19.86
1.5	704	575	528	372	156	0.88	0.52	19.70
2	708	580	531	375	156	0.88	0.52	20.3

Additionally, the number of bonds per unit volume of the glass can be calculated using the relation [31],

$$n_b = \frac{N_A}{V_m} m, \quad (7)$$

where the average coordination number of the glass, m is given by

$$m = \sum_i CN_i X_i. \quad (8)$$

CN_i represents the coordination number of the cations that are directly obtained from the literature [32]. It can be seen that the number of bonds per unit volume of glasses is decreasing with increasing concentration of Er_2O_3 which confirms the kind of variation observed in the molar volume and density values.

3.2.3 Erbium ion concentration, internuclear distance, field strength, and polaron radius

The concentration of Er^{3+} ions (N_{Er}), field strength (F), polaron radius (r_{pn}) and internuclear distance (d) are calculated using appropriate formulae [33] and registered in Table 2. The values of polaron radius (r_{pn}) and internuclear distance (d) are found to be decreasing with increased Er^{3+} content in all the glass samples indicating the rise in Er-O bond strength which produces the strong field strength around Er^{3+} ions. Variation of internuclear distance and polaron radius with concentration of erbium ions is shown in Fig. 4.

3.3 Thermal properties

Differential thermal analysis is a well-known and an appropriate method for the evaluation of characteristic temperatures of any glass like glass transition, crystallization, and melting temperature [16]. These thermal characteristics are necessary for the determination of thermal stability and glass forming ability of any glass. DTA curves obtained at the heating rate of 10 °C/min for PZLE0 and PZLE10

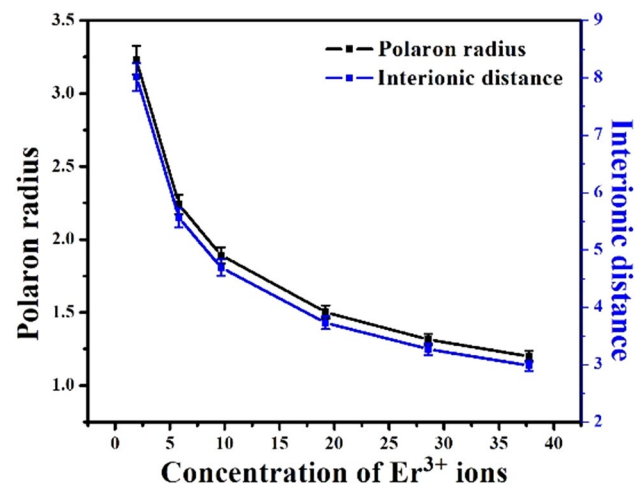


Fig. 4 Variation of polaron radius and interionic distance with concentration of Er^{3+} ions

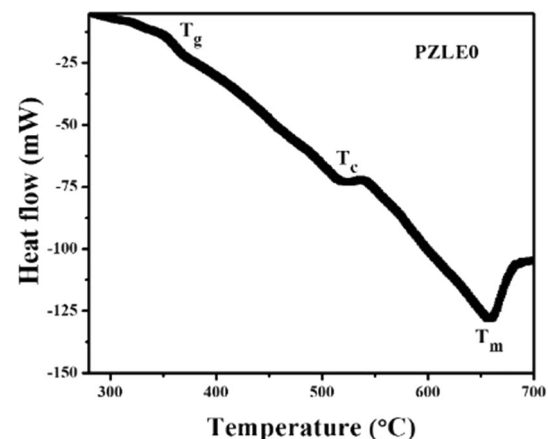


Fig. 5 DTA curve of PZLE0 glass sample

glasses are portrayed in Figs. 5 and 6. A distinct peak is observed owing to T_g in the obtained DTA curves indicating the homogeneity of the glasses. All the determined thermal parameters are given in Table 2. The glass transition temperature for the glass samples is in the range 356–375 °C. The

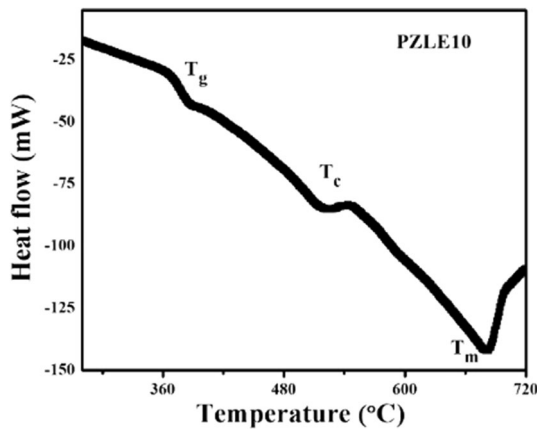


Fig. 6 DTA curve of PZLE10 glass sample

thermal stability of the glasses can be analysed by calculating the difference between onset crystallization temperature, T_c and the glass transition temperature, T_g [34] i.e.,

$$T_S = T_c - T_g. \quad (9)$$

Glass forming ability, K is calculated using the relation given by Hrubby [35, 36],

$$K = \frac{T_c - T_g}{T_m - T_c}. \quad (10)$$

The higher values of $(T_c - T_g)$ indicates the delay in nucleation activity and the smaller values of $(T_m - T_c)$ hold up the growing of the nucleated crystals [37].

The ability of glass formation is usually evaluated by finding the reduced glass transition temperature (T_{rg}) of the glass [38, 39]. Here, we see that the values obtained for all the glasses are obeying the two-thirds rule, which states that

$$T_{rg} = \frac{T_g}{T_m}, \quad (11)$$

such that $\frac{1}{2} \leq T_{rg} \leq \frac{2}{3}$. The thermal stability parameter which reveals the opposition offered by the glass formed to crystallization, introduced by Saad and Poulin [40] can also be calculated using

$$S = \frac{(T_p - T_c)(T_c - T_g)}{T_g}. \quad (12)$$

$(T_p - T_c)$ indicates the rate of crystallization from the glassy state [41, 42]. All the calculated values of T_S , S , T_{rg} and K for different concentration of Er³⁺ are listed in Table 2. These results from the data obtained indicate that the prepared glass samples have good thermal stability as specified by all the calculated glass stability factors and,

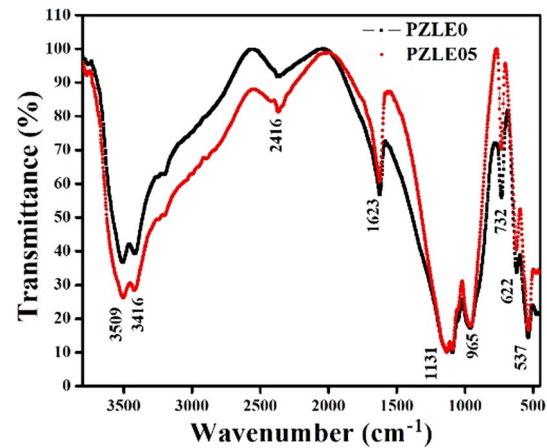


Fig. 7 FTIR spectra of un-doped and 0.5 mol% of rare earth doped PZL glasses

therefore, these glasses can be good materials for fibre fabrication.

3.4 Structural properties (FTIR study)

FTIR spectra of Er³⁺ doped and undoped PZL glasses are recorded and we observe that they all show alike spectral characteristics. Figure 7 shows spectra of 0.5 mol% of Er³⁺ doped and un-doped PZL glass matrices. The spectrum consists of nine bands at ~ 537 cm⁻¹, ~ 622 cm⁻¹, ~ 732 cm⁻¹, ~ 965 cm⁻¹, ~ 1131 cm⁻¹, ~ 1623 cm⁻¹, ~ 2416 cm⁻¹, ~ 3416 cm⁻¹ and ~ 3509 cm⁻¹. The well-known fact is that the cross-linking PO₄ tetrahedra with three bridging oxygen and a terminal double bonded oxygen constitute the network of phosphate glasses. Here, the absorption band observed at 537 cm⁻¹ may be consigned to the bending modes of P–O in PO₄. Band at 622 cm⁻¹ is due the Zn–O stretching vibration of the ZnO₄ unit. 732 cm⁻¹ indicates the presence of meta-phosphate groups and it can be allocated to symmetric stretching vibrations of bridging oxygen. The band at 965 cm⁻¹ can be assigned to the asymmetric stretching mode of P–O–P linkages and band at 1131 cm⁻¹ is a characteristic band due to the asymmetric stretching vibrations of non-bridging oxygen atoms bonded to phosphorus atom, i.e., O–P–O. Around 1623 cm⁻¹ the band observed is because of the stretching and bending vibrations of P–O–H bridges and water which is because of the absorption of moisture. It is observed that there is a gradual decrease in the intensity of the band at 1623 cm⁻¹ which indicates the decrease of hygroscopic nature of the glasses. Vibrational band at 2416 cm⁻¹ is due to the hydrogen bond between P–OH and O–Zn units. The band around 3416 cm⁻¹ and 3509 cm⁻¹ specifies the presence of hydrogen bonding and O–H stretching vibration respectively [43–50].

3.5 Optical properties

3.5.1 Optical absorption, Urbach energy and energy band gap

Figure 8 shows UV–visible absorption spectra of the glasses containing 0.3 mol% and 1.5 mol% of Er_2O_3 . It comprises eleven prominent and sharp absorption peaks. All the peaks instigate from ground state $^4\text{I}_{15/2} \rightarrow ^2\text{G}_{7/2}$ (255 nm), $^4\text{G}_{9/2}$ (364 nm), $^4\text{G}_{11/2}$ (377 nm), $^2\text{G}_{9/2}$ (407 nm), $^4\text{F}_{5/2}$ (451 nm), $^4\text{F}_{7/2}$ (489 nm), $^2\text{H}_{11/2}$ (522 nm), $^4\text{S}_{3/2}$ (545 nm), $^4\text{F}_{9/2}$ (656 nm), $^4\text{I}_{9/2}$ (800 nm) and $^4\text{I}_{11/2}$ (980 nm) [51–54]. All these transitions well agree with the previously measured absorption data available in the literature for Er_2O_3 doped glasses and they obey $\Delta S=0$, $\Delta L \leq 0$ and $\Delta J \leq 0$ selection rules [55]. The intensity of the absorption peaks is found to be increasing with the increasing concentration of Er_2O_3 indicating the good rare earth solubility of the prepared glass matrix.

The electronic band structure of glasses and transitions which happen between valence and conduction band can be studied and understood from the absorption spectra measured in the UV–visible region. The direct/indirect energy difference between the conduction and the valence band is the optical energy band gap, an important means to explain the structure and characteristics of the material. It can be enumerated using the following equation described by Davis and Mott [56],

$$\alpha h\nu = B(h\nu - E_{\text{opt}})^r, \quad (13)$$

where

$$\alpha(\lambda) = 2.303 \frac{A}{d}, \quad (14)$$

is the optical absorption coefficient which depends on the thickness, d and absorbance, A of the glass, $h\nu$ represents the

photon energy, r is a number which depends on the kind of transition taking the values 2, 3, $1/2$ and $3/2$ corresponding to indirect allowed, indirect forbidden, direct allowed and direct forbidden transition respectively, B is a constant which represents the band tailing parameter. Both indirect and direct bandgap values were determined from Tauc's plots, i.e., $(\alpha h\nu)^{1/2}$ versus $h\nu$ and $(\alpha h\nu)^2$ versus $h\nu$ plots, as shown in Figs. 9 and 10 by extending the linear part of the curve to the x -axis. $(\alpha h\nu)^2=0$ and $(\alpha h\nu)^{1/2}=0$ for direct and indirect transition, respectively. It is seen that direct bandgap values lie between 4.230 and 4.042 eV and indirect bandgap values lie between 3.976 and 3.576 eV (Table 3). Decrease in indirect and direct bandgap energies with increasing Er_2O_3 and decreasing Li_2O content is observed. This decrease is the outcome of the generation of non-bridging oxygen and the changes that may have taken place in the bonds.

Amorphous substances have trailing of the density of states into the bandgap and width of these band tails is termed as Urbach energy (ΔE) [57]. It is the measure of

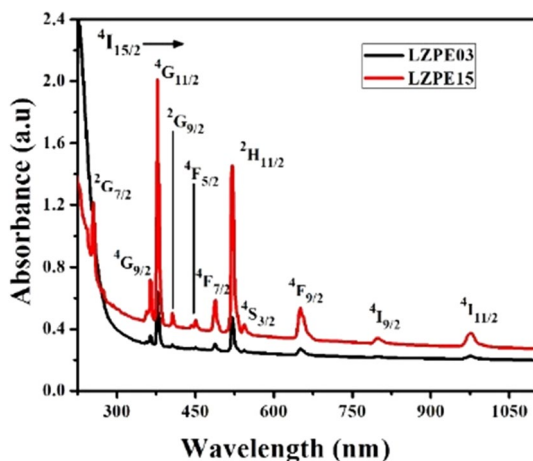


Fig. 8 UV–Vis absorption spectra of PZL glasses with 0.3 mol% and 1.5 mol% of Er_2O_3

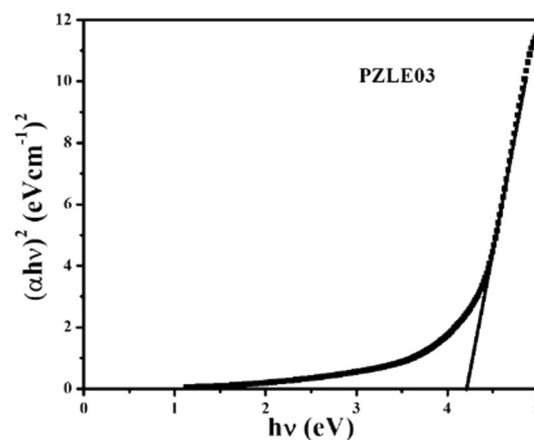


Fig. 9 Plot of $(\alpha h\nu)^2$ versus $h\nu$ for PZLE03 glass sample

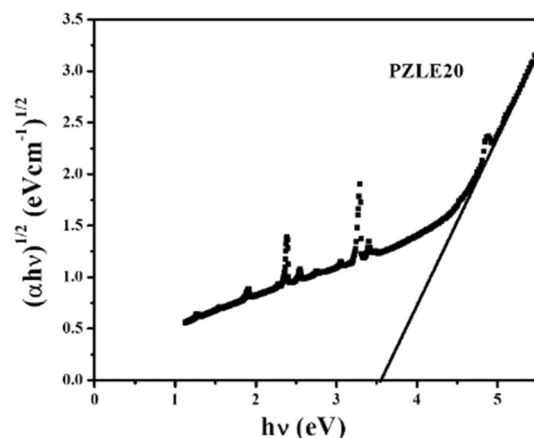
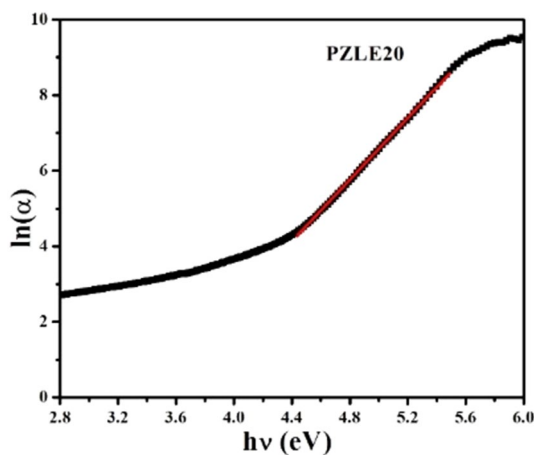


Fig. 10 Plot of $(\alpha h\nu)^{1/2}$ versus $h\nu$ for PZLE20 glass sample

Table 3 Optical direct and indirect bandgap— $E_{g(d)}$, $E_{g(ind)}$ (eV), Urbach energy— ΔE (eV), steepness parameter— S , refractive index— n , dielectric constant— n^2 , reflection loss— R_L (%), molar refraction— R_m (cm³/mol), molar polarizability— α_m (Å³) and metallization criterion (M)

x (mol%)	$E_{g(d)}$ ± 0.001	$E_{g(ind)}$ ± 0.001	ΔE ± 0.001	S ± 0.0001	n ± 0.001	n^2 ± 0.001	R_L ± 0.001	R_m ± 0.001	α_m ± 0.001	M ± 0.0001
0	4.230	3.976	0.471	0.0545	1.590	2.528	5.189	10.448	4.146	0.6625
0.1	4.202	3.791	0.504	0.0509	1.593	2.537	5.230	10.501	4.167	0.6611
0.3	4.191	3.713	0.523	0.0491	1.595	2.544	5.257	10.553	4.187	0.6602
0.5	4.164	3.693	0.541	0.0474	1.596	2.547	5.270	10.592	4.203	0.6597
1	4.105	3.674	0.563	0.0456	1.597	2.550	5.284	10.684	4.239	0.6593
1.5	4.066	3.609	0.589	0.0435	1.598	2.553	5.298	10.778	4.280	0.6588
2	4.042	3.576	0.594	0.0422	1.600	2.560	5.325	10.909	4.328	0.6579

**Fig. 11** $\ln(\alpha)$ as a function of $h\nu$ for PZLE20 glass sample

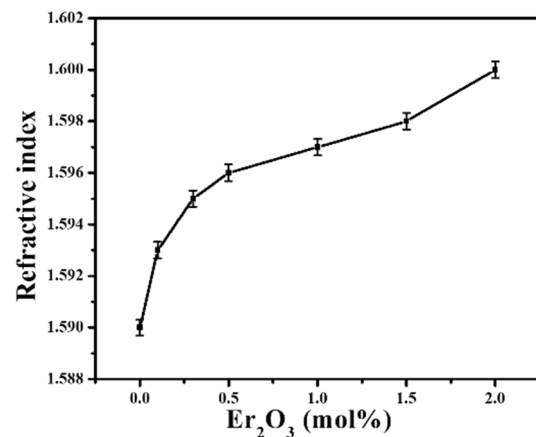
disorderness in the crystalline as well as non-crystalline materials. ΔE can be determined using the following equation,

$$\ln \alpha = \ln \alpha_o + \frac{h\nu}{\Delta E}, \quad (15)$$

by plotting a graph of $\ln(\alpha)$ versus $h\nu$ and taking the reciprocal of the slope of the linear region of the curves as shown in Fig. 11. Here ΔE values are increasing with increase in the Er_2O_3 content indicating the increased disorderness in the glass structure which may be due to the presence of structural defects. ΔE values for these glasses well agree and follow the fact that smaller the bandgap energy greater will be the Urbach energy. Steepness parameter (S) [58] at room temperature for the samples can be determined by the formula,

$$S = \frac{kT}{\Delta E} \quad (16)$$

where T is the room temperature and k is Boltzmann constant.

**Fig. 12** Variation of refractive index with Er_2O_3 concentration

3.5.2 Molar polarizability, refractive index, and molar refraction

On addition of Er_2O_3 , the refractive index of the glasses is increasing from 1.590 to 1.60 due to the fact that, Er^{3+} with highest coordination number 6 than any other components in the matrix play as a network modifier increasing NBO bonds in the matrix. The behaviour of the refractive index with Er_2O_3 content is shown in Fig. 12.

Molar refraction and the molar polarizability denoted by R_m and α_m , respectively, are calculated from the obtained molar volume and refractive index values using Lorentz–Lorentz equation [33]

$$R_m = \frac{n^2 - 1}{n^2 + 2} V_m, \quad (17)$$

$$\alpha_m = \frac{R_m}{2.52}. \quad (18)$$

Both molar refraction and polarizability are found to be increasing with increasing concentration of Er_2O_3 as it can be seen from Fig. 13.

Reflection loss (R_L), dielectric constant (ϵ) of all the glass samples are evaluated from the corresponding refractive index values using the following relations,

$$\epsilon = n^2, \quad (19)$$

$$R_L = \left(\frac{n-1}{n+1} \right)^2 \times 100. \quad (20)$$

Metallic or non-metallic nature of any material can be identified by calculating the metallization criterion [59] given by,

$$M = 1 - \frac{V_m}{R_m}. \quad (21)$$

If $R_m > V_m$, the materials are said to be metallic and they are insulators if $R_m < V_m$. Here, we can see that all the prepared glass samples show insulating nature.

The variation observed in all these parameters on adding Er^{3+} ions is mainly because of the creation of additional non-bridging oxygens.

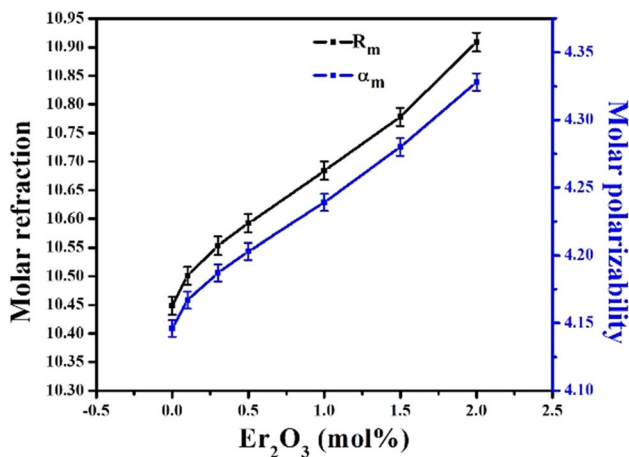


Fig. 13 Variation of molar refraction and molar polarizability with Er_2O_3 concentration

3.5.3 Optical basicity, interaction parameter and electronic polarizability of oxide ions

Electronic oxide polarizability [60] based on the obtained refractive index values can be evaluated from the equation given by:

$$\alpha_{\text{O}^{2-}} = \left[\left(\frac{V_m}{2.52} \right) \left(\frac{n^2-1}{n^2+2} \right) - \sum \alpha_{\text{cat}} \right] / N_{\text{O}^{2-}} \quad (22)$$

where $\sum \alpha_{\text{cat}}$ denotes the molar cation polarizability, $N_{\text{O}^{2-}}$ represents the number of oxide ions and $\alpha_{\text{O}^{2-}}$ represents the electronic oxide polarizability of the glass sample. For any glass $x\text{A}_a\text{O}_b - y\text{B}_c\text{O}_d - z\text{C}_e\text{O}_f - t\text{D}_g\text{O}_h$, $\sum \alpha_{\text{cat}}$ will be $x\alpha_{\text{A}} + y\alpha_{\text{B}} + z\alpha_{\text{C}} + t\alpha_{\text{D}}$ and $N_{\text{O}^{2-}}$ will be $xb + yd + zf + th$. Here α_{p} , α_{Zn} , α_{Li} and α_{Er} values are taken from the literature [61] and the calculated $\alpha_{\text{O}^{2-}}$ and $N_{\text{O}^{2-}}$ values are tabulated in Table 4. We can see that $\alpha_{\text{O}^{2-}}$ values calculated based on refractive index are increasing with the rise in Er^{3+} ions concentration as expected. The variation of electronic polarizability with Er^{3+} ions concentration is shown in Fig. 14.

Optical basicity of any glass refers to the ability of that glass to donate negative charge of the ion [62, 63]. It can be calculated from electronic oxide polarizability using the following relation [64]:

$$\Lambda = 1.67 \left(1 - \frac{1}{\alpha_{\text{O}^{2-}}} \right). \quad (23)$$

The relationship between the electronic polarizability and the optical basicity of glasses is shown in Fig. 15.

Theoretical optical basicity of the prepared glass samples can be determined using the following relation:

$$\Lambda_{\text{th}} = X_{\text{Er}_2\text{O}_3} \Lambda_{\text{Er}_2\text{O}_3} + X_{\text{P}_2\text{O}_5} \Lambda_{\text{P}_2\text{O}_5} + X_{\text{Li}_2\text{O}} \Lambda_{\text{Li}_2\text{O}} + X_{\text{ZnO}} \Lambda_{\text{ZnO}}, \quad (24)$$

where $X_{\text{Er}_2\text{O}_3}$, $X_{\text{P}_2\text{O}_5}$, $X_{\text{Li}_2\text{O}}$ and X_{ZnO} are the equivalent fractions based on the amount of oxygen and $\Lambda_{\text{Er}_2\text{O}_3}$, $\Lambda_{\text{P}_2\text{O}_5}$, $\Lambda_{\text{Li}_2\text{O}}$ and Λ_{ZnO} are the optical basicity of the corresponding oxides and they are obtained from the literature [61, 65]. From the calculated values, we observe that

Table 4 Electronic polarizability of oxide ions ($\alpha_{\text{O}^{2-}}$), number of oxide ions ($N_{\text{O}^{2-}}$), optical basicity (Λ), theoretical optical basicity (Λ_{th}), electronegativity (χ), electric susceptibility (χ_e), interaction parameter (A) and theoretical interaction parameter (A_{th})

x (mol%)	$\alpha_{\text{O}^{2-}}$ (\AA^3) ± 0.001	$N_{\text{O}^{2-}}$ ± 0.001	Λ ± 0.001	Λ_{th} ± 0.001	χ ± 0.0001	χ_e ± 0.0001	A (\AA^{-3}) ± 0.0001	A_{th} (\AA^{-3}) ± 0.0001
0	1.5364	2.6	0.5830	0.5911	1.0381	0.1216	0.1962	0.1963
0.1	1.5427	2.602	0.5874	0.5920	1.0393	0.1223	0.1961	0.1961
0.3	1.5470	2.606	0.5904	0.5931	1.0408	0.1228	0.1958	0.1959
0.5	1.5491	2.61	0.5925	0.5943	1.0424	0.1231	0.1955	0.1956
1	1.5539	2.62	0.5953	0.5974	1.0465	0.1233	0.1949	0.1950
1.5	1.5603	2.63	0.5996	0.6005	1.0506	0.1236	0.1943	0.1944
2	1.5694	2.64	0.6056	0.6034	1.0545	0.1241	0.1936	0.1937

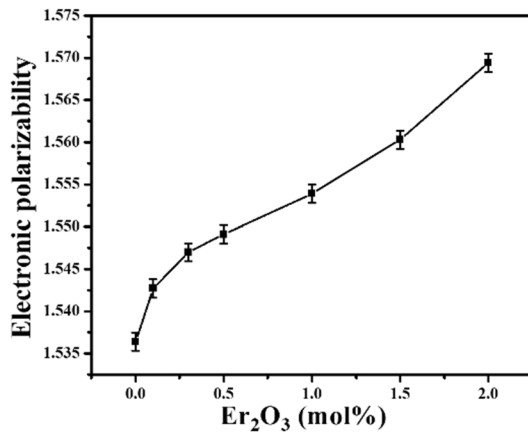


Fig. 14 Variation of electronic polarizability with Er₂O₃ concentration

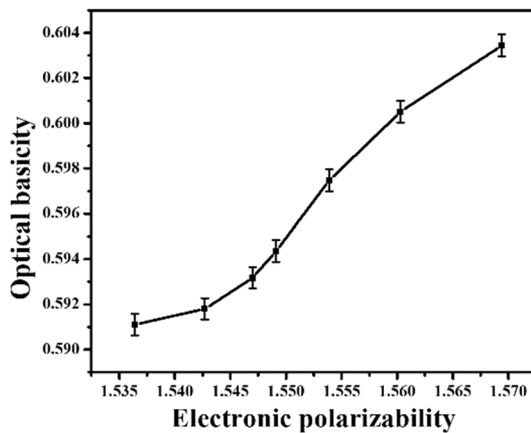


Fig. 15 Relationship between electronic polarizability and optical basicity

with an increase in the Er₂O₃ content optical basicity is also increasing indicating that the glasses are capable of donating a negative charge to the surrounding cation leading to an increased covalency of the oxygen-cation bonds.

Electronegativity and electric susceptibility [65, 66] are also calculated using the relations given below,

$$\chi = \frac{\Lambda}{0.75} + 0.25 \quad (25)$$

$$\chi_e = \frac{(n^2 - 1)}{4\pi} \quad (26)$$

Interaction parameter of glasses describes the polarizability state of an oxide ion in oxides and also the ability to form an ionic covalent bond with the cation [67]. From Dimitrov and Komatsu equation [68] (modified Yamashita and Kurosawa equation [69]) for interaction parameter of

simple oxides, interaction parameter can be determined using:

$$A = X_{\text{Er}_2\text{O}_3} \frac{(3.921 - \alpha_{\text{O}^{2-}})}{2(\alpha_{\text{Er}^{3+}} + 3.921)(\alpha_{\text{Er}^{3+}} + \alpha_{\text{O}^{2-}})} + X_{\text{P}_2\text{O}_5} \frac{(3.921 - \alpha_{\text{O}^{2-}})}{2(\alpha_{\text{P}^{5+}} + 3.921)(\alpha_{\text{P}^{5+}} + \alpha_{\text{O}^{2-}})} + X_{\text{Li}_2\text{O}} \frac{(3.921 - \alpha_{\text{O}^{2-}})}{2(\alpha_{\text{Li}^{2+}} + 3.921)(\alpha_{\text{Li}^{2+}} + \alpha_{\text{O}^{2-}})} + X_{\text{ZnO}} \frac{(3.921 - \alpha_{\text{O}^{2-}})}{2(\alpha_{\text{Zn}^{2+}} + 3.921)(\alpha_{\text{Zn}^{2+}} + \alpha_{\text{O}^{2-}})} \quad (27)$$

Values for polarizabilities of oxide ions and free cations are used from literature [61, 65] to calculate the interaction parameter.

Theoretical interaction parameter of the glasses is calculated using the formula [70],

$$A_{\text{th}} = X_{\text{Er}_2\text{O}_3} A_{\text{Er}_2\text{O}_3} + X_{\text{P}_2\text{O}_5} A_{\text{P}_2\text{O}_5} + X_{\text{Li}_2\text{O}} A_{\text{Li}_2\text{O}} + X_{\text{ZnO}} A_{\text{ZnO}}, \quad (28)$$

where $A_{\text{Er}_2\text{O}_3}$, $A_{\text{P}_2\text{O}_5}$, $A_{\text{Li}_2\text{O}}$ and A_{ZnO} are the interaction parameters of corresponding oxides and their values are taken from literature [68] and the value of $A_{\text{Er}_2\text{O}_3}$ is calculated using Dimitrov and Komatsu equation. Calculated values of A and A_{th} are tabulated in Table 4.

It is found that the calculated interaction parameter is decreasing with increasing concentration of Er₂O₃ which is in total agreement with the fact that larger the optical basicity smaller will be the interaction parameter. Variation of the calculated theoretical optical basicity and interaction parameter with Er₂O₃ concentration is shown in Fig. 16.

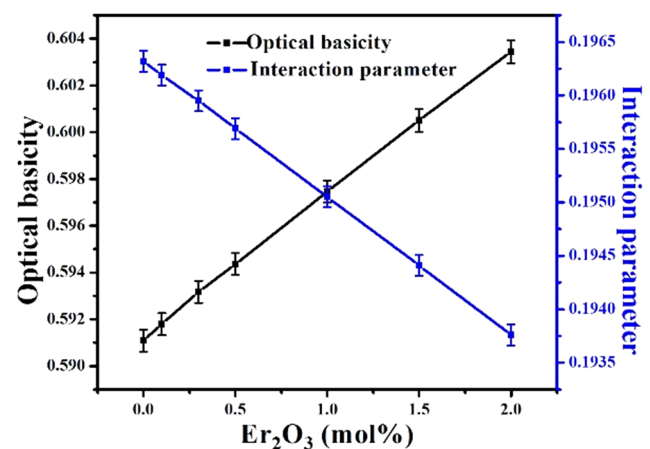


Fig. 16 Variation of theoretical optical basicity and theoretical interaction parameter with Er₂O₃ concentration

4 Conclusion

Er₂O₃ doped zinc lithium phosphate glass samples were synthesized by simple and conservative melt quenching method. Non-crystalline nature of the prepared glasses was confirmed by the obtained XRD patterns. On increasing the rare earth oxide concentration density and the molar volume of the glass were found to be increasing due to the non-bridging oxygen and the decreased packing density and OPD. FTIR studies show the structural units and the functional groups present in the glass samples. Additionally, the very few OH groups observed in the spectra point out the chance of improvement in the luminescence of glasses. The dependency of the melting (T_m), crystallization (T_p), and glass transition (T_g) temperatures on the concentration of Er₂O₃ were examined by DTA studies. The glass stability factor ($T_c - T_g$) of the glass system is found to be greater than 100 °C, which is a necessary condition to achieve fibre drawing. Additionally, these glasses have higher values of Hruby's parameter and hence these glasses possess greater glass forming tendency. Briefly, the obtained results from the data indicate a good thermal stability of the prepared glasses and, therefore, these glasses can find application in fibre fabrication. The optical bandgap is found to be decreasing with increasing concentration of Er₂O₃ which is due to the shifting of absorption edge to a region of longer wavelength. Refractive index, electronic polarizability, and optical basicity of the glasses are found to increase with increasing Er₂O₃ content while the interaction parameter is found to be decreasing which can be ascribed to the non-bridging oxygen. These overall studies and the obtained results imply that the prepared glasses find potential applications in developing display devices, thermal sensors and also can be good materials for fibre fabrication.

References

1. Z. Pan, S.H. Morgan, K. Dyer, A. Ueda, Host dependent optical transitions of Er³⁺ ions in lead-germanate and lead tellurium germanate glasses. *J. Appl. Phys.* **79**, 8906–8913 (1996)
2. J. Fernandez, I. Iparraguirre, R. Balda, J. Azkargorta, M. Voda, J.M. Fernandez-Navarro, Laser action and upconversion of Nd³⁺ in lead-niobium-germanate bulk glass. *Opt. Mater.* **25**, 185–191 (2004)
3. T.P. Tang, C.M. Lee, F.C. Yen, The photoluminescence of SrAl₂O₄: Sm phosphors. *Ceram. Int.* **32**, 665–671 (2006)
4. G.M. Kumar, B.N.S. Bhaktha, D.N. Rao, Self-quenching of spontaneous emission in Sm³⁺ doped lead-borate glass. *Opt. Mater.* **28**, 1266–1270 (2006)
5. W.A. Pisarski, J. Pisarska, R. Lisiecki, Up-conversion processes of rare earth ions in heavy metal glasses. *J. Rare Earths* **29**, 1192–1194 (2011)
6. S. Tanabe, Fluorescence properties of Er³⁺ ions in glass ceramics containing LaF₃ nanocrystals. *Opt. Mater.* **19**(3), 343–349 (2002)
7. A. Mogus-Milankovic, V. Licina, S.T. Reis, D.E. Day, Electronic relaxation in zinc iron phosphate glasses. *J. Non Cryst. Solids* **353**, 2659–2666 (2007)
8. S.N. Sdiri, H. Elhouichet, C. Barthou, M. Ferid, Spectroscopic properties of Er³⁺ and Yb³⁺ doped phosphate-borate glasses. *J. Mol. Struct.* **1010**, 85–90 (2012)
9. S. Jiang, T. Luo, B.C. Hwang, F. Smekatala, K. Seneschal, J. Lucas, N. Peyghambarian, Er³⁺ doped phosphate glasses for fiber amplifiers with high gain per unit length. *J. Non Cryst. Solids* **263/264**, 364–368 (2000)
10. J.A. Caird, A.J. Romponi, P.R. Staves, Quantum efficiency and excited-state relaxation dynamics in neodymium-doped phosphate laser glasses. *J. Opt. Soc. Am. B* **8**, 1391–1403 (1991)
11. M.I. Abd El-Ati, A.A. Higazy, Electrical conductivity and optical properties of gamma-irradiated niobium phosphate glasses. *J. Mater. Sci.* **35**, 6175–6180 (2000)
12. X.C. Yu, F. Song, W.T. Wang, L.J. Luo, C.G. Ming, Effects of Ce³⁺ on the spectroscopic properties of transparent phosphate glass ceramics co-doped with Er³⁺/Yb³⁺. *Opt. Commun.* **282**, 2045–2048 (2009)
13. J. Wang, H. Song, X. Kong, H. Peng, B. Sun, B. Chen, J. Zhang, W. Xu, H. Xia, Fluorescence properties of trivalent europium doped in various niobate codoped glasses. *J. Appl. Phys.* **93**, 1482–1486 (2003)
14. Z. Lin, C. Qi, S. Dai, Y. Jiang, L. Hu, Spectra and laser properties of Er³⁺, Yb³⁺: phosphate glasses. *Opt. Mater.* **21**, 789–794 (2003)
15. T.I. Suratwala, R.A. Steele, G.D. Wike, J.H. Campbell, K. Takenchi, Effects of OH content, water vapor pressure, and temperature on sub-critical crack growth in phosphate glass. *J. Non Cryst. Solids* **263/264**, 213–227 (2000)
16. P. Pascuta, M. Bosca, G. Borodi, E. Culea, Thermal, structural and magnetic properties of some zinc phosphate glasses doped with manganese ions. *J. Alloys Compd.* **509**, 4314–4319 (2011)
17. C.E. Smith, R.K. Brow, The properties and structure of zinc magnesium phosphate glasses. *J. Non Cryst. Solids* **390**, 51–58 (2014)
18. K. Aida, T. Komatsu, V. Dimitrov, Thermal stability, electronic polarizability and optical basicity of ternary tellurite glasses. *Phys. Chem. Glasses* **42**(2), 103–111 (2001)
19. P.W. McMillan, *Glass Ceramics*, 2nd edn. (Academic, London, 1979)
20. N.A. Ghoniem, H.A. Elbatal, A.M. Abdelghany, I.S. Ali, Shielding behavior of V₂O₅ doped lead borate glasses towards gamma irradiation. *J. Alloys compd.* **509**, 6913–6919 (2011)
21. Y.B. Peng, D.E. Day, Y.B. Peng, D.E. Day, High thermal expansion phosphate glasses. Part I. *Glass Technol.* **32**, 166–173 (1991)
22. W.J. Chung, A. Jha, S. Shen, P. Joshi, The effect of Er³⁺-ion concentration on the Er³⁺:⁴I_{13/2}→⁴I_{15/2} transition in tellurite glasses. *Philos. Mag.* **84**, 1197–1207 (2004)
23. G.A. Kumar, E. DelaRosa, H. Desirena, Radiative and non-radiative spectroscopic properties of Er³⁺ ion in tellurite glass. *Opt. Commun.* **260**, 601–606 (2006)
24. H. Chen, Y.H. Liu, Y.F. Zhou, Z.H. Jiang, Spectroscopic properties of Er³⁺-doped tellurite glass for 1.55 μm optical amplifier. *J. Alloys Compd.* **397**, 286–290 (2005)
25. R. Rolli, M. Montagna, S. Chaussedent, A. Monteil, V.K. Tikhomirov, M. Ferrari, Erbium-doped tellurite glasses with high quantum efficiency and broadband stimulated emission cross section at 1.5 μm. *Opt. Mater.* **21**, 743–748 (2003)
26. S. Hu, Z. Yang, S. Dai, G. Wang, L. Hu, Z. Jiang, Effect of Bi₂O₃ on spectroscopic properties of Er³⁺-doped lead oxyfluorosilicate glasses for broadband optical amplifiers. *J. Non Cryst. Solids* **347**, 197–203 (2004)
27. N.F. Mott, E.A. Davis, *Electronic Process in the Non-crystalline Materials*, 2nd edn. (Clarendon Press/Oxford University, New York, 1979)

28. V.C. Veeranna Gowda, Effect of Bi³⁺ ions on physical, thermal, spectroscopic and optical properties of Nd³⁺ doped sodium diborate glasses. *Physica B* **426**, 58–64 (2013)
29. S. Inaba, S. Fujino, K. Morinaga, Young's modulus and compositional parameters of oxide glasses. *J. Am. Ceram. Soc.* **82**, 3501–3507 (1999)
30. M.A. Algrade, A. Elwhab, B. Alwany, M. Sultan, M. Elgoshimy, Q. Almoraisy, Physical and optical properties for Nd₂O₃ doped lithium–zinc–phosphate glasses. *Optik* **142**, 13–22 (2017)
31. M. Abdel-Baki, F.A. Abdel-Wahab, F. El-Diasty, One-photon band gap engineering of borate glass doped with ZnO for photonics applications. *J. Appl. Phys.* **111**, 073506–073510 (2012)
32. D.R. Lide (ed.), *CRC Handbook of Chemistry and Physics*, 85th edn. (CRC Press, Boca Raton, 2004)
33. J.E. Shelby, Properties and structure of lithium germinate glasses. *Phys. Chem. Glasses* **28**(6), 262–268 (1987)
34. B. Karthikeyan, S. Mohan, Structural, optical and glass transition studies on Nd³⁺-doped lead bismuth borate glasses. *Phys. B* **334**, 298–302 (2003)
35. A. Hruby, Evaluation of glass-forming tendency by means of DTA. *Czech. J. Phys. B* **22**(11), 1187–1193 (1972)
36. A. Hruby, Glass-forming tendency in the GeS_x system. *Czech. J. Phys. B* **23**(11), 1263–1272 (1973)
37. V. Kumar, S. Sharma, O.P. Pandey, K. Singh, Thermal and physical properties of 30SrO–40SiO₂–20B₂O₃–10A₂O₃ (A = La, Y, Al) glasses and their chemical reaction with bismuth vanadate for SOFC. *Solid State Ionics* **181**, 79–85 (2010)
38. W. Kauzmann, The nature of the glassy state and the behavior of liquids at low temperatures. *Chem. Rev.* **43**, 219–256 (1948)
39. M.T. Clavaguera-Mora, Glassy materials: thermodynamic and kinetic quantities. *J. Alloys Compd.* **220**, 197–205 (1995)
40. M. Saad, M. Poulin, Glass forming ability criterion. *Mater. Sci. Forum* **19–20**, 11–18 (1987)
41. N. Mehta, R.S. Tiwari, A. Kumar, Glass forming ability and thermal stability of some Se–Sb glassy alloys. *Mater. Res. Bull.* **41**, 1664–1672 (2006)
42. E.R. Shaaban, I.S. Yahia, M. Fadel, Effect of composition on the thermal stability for Ge–In–Se intermediate compound. *J. Alloys Compd.* **469**, 427–432 (2009)
43. P.Y. Shih, Properties and FTIR spectra of lead phosphate glasses for nuclear waste immobilization. *Mater. Chem. Phys.* **80**, 299–304 (2003)
44. L. Montagne, G. Palavit, G. Mairesse, 31P MAS NMR and FTIR analysis of (50 – x/2) Na₂O · xBi₂O₃ · (50 – x/2) P₂O₅ glasses. *Phys. Chem. Glasses* **37**, 206–211 (1996)
45. H.S. Liu, T.S. Chin, S. W. Yung, FTIR and XPS studies of low-melting PbO–ZnO–P₂O₅ glasses. *Mater. Chem. Phys.* **50**, 1–10 (1997)
46. J.O. Byun, B.H. Kim, K.S. Hong, H.J. Jung, S.W. Lee, A.A. Izyneev, Properties and structure of RO–Na₂O–Al₂O₃–P₂O₅ (R = Mg, Ca, Sr, Ba) glasses. *J. Non Cryst. Solids* **190**, 288–295 (1995)
47. A.A. El-Kheshen, F.A. Khaliifa, E.A. Saad, R.L. Elwan, Effect of Al₂O₃ addition on bioactivity, thermal and mechanical properties of some bioactive glasses. *Ceram. Int.* **34**, 1667–1673 (2008)
48. M.A. Marzouk, H.A. ElBatal, A.M. Abdel Ghany, F.M. Ezz Eldin, Ultraviolet, visible, ESR, and infrared spectroscopic studies of CeO₂-doped lithium phosphate glasses and effect of gamma irradiation. *J. Mol. Struct.* **997**, 94–102 (2011)
49. M.A. Ouis, H.A. El-Batal, M.A. Azooz, A.M. Abdelghany, Characterization of WO₃-doped borophosphate glasses by optical, IR and ESR spectroscopic techniques before and after subjecting to gamma irradiation. *Indian J. Pure Appl. Phys.* **51**, 11–17 (2013)
50. Y.M. Lai, X.F. Liang, S.Y. Yang, J.X. Wang, L.H. Cao, B. Dai, Raman and FTIR spectra of iron phosphate glasses containing cerium. *J. Mol. Struct.* **992**, 84–88 (2011)
51. Y.L. Ruijie Cao, Y. Tian, F. Huang, Y. Guo, S. Xu, J. Zhang, Spectroscopy of thulium and holmium co-doped silicate glasses. *Opt. Mater. Express* **6**(7), 2252–2263 (2016)
52. W.T. Carnall, P.R. Field, K. Rajnak, Electronic energy levels in the trivalent lanthanide aquo ions. I. Pr³⁺, Nd³⁺, Pm³⁺, Sm³⁺, Dy³⁺, Ho³⁺, Er³⁺ and Tm³⁺. *J. Chem. Phys.* **49**, 4424–4442 (1968)
53. N. Vijaya, P. Babu, V. Venkatramu, C.K. Jayasankar, S.F. León-Luis, U.R. Rodríguez-Mendoza, I.R. Martín, V. Lavín, Optical characterization of Er³⁺-doped zinc fluorophosphate glasses for optical temperature sensors. *Sens. Actuators B* **186**, 156–164 (2013)
54. K. Jorgenson, B.R. Judd, Hypersensitive pseudoquadrupole transitions in lanthanides. *Mol. Phys.* **8**, 281–290 (1964)
55. H.A.A. Sidek, I.T. Collier, R.N. Hampton, G.A. Saunders, B. Bridge, Electrical conductivity and dielectric constant of samarium phosphate glasses. *Philos. Mag. B* **59**, 221–232 (1989)
56. E.A. Davis, N.F. Mott, Conduction in non-crystalline systems V. Conductivity, optical absorption and photoconductivity in amorphous semiconductors. *J. Philos. Mag.* **22**, 903–922 (1970)
57. F. Urbach, The long-wavelength edge of photographic sensitivity and of the electronic absorption of solids. *Phys. Rev.* **92**, 1324–1324 (1953)
58. H. Mahr, Ultraviolet absorption of KI diluted in KCl crystals. *Phys. Rev.* **125**, 1510–1516 (1962)
59. S.L.S. Rao, G. Ramadevudu, M. Shareefuddin, A. Hameed, M.N. Chary, M.L. Rao, Optical properties of alkaline earth borate glasses. *Int. J. Eng. Sci. Technol.* **4**, 25–35 (2012)
60. T.S. Moss, Relations between the refractive index and energy gap of semiconductors. *Phys. Stat. Solidi (b)* **131**, 415–427 (1985)
61. X. Zhao, X. Wang, H. Lin, Z. Wang, Electronic polarizability and optical basicity of lanthanide oxides. *Phys. B* **392**, 132–136 (2007)
62. S.S. Sastry, B.R. Venkateswara Rao, Structural and optical properties of vanadium doped alkaline earth lead zinc phosphate glasses. *Indian J. Pure Appl. Phys.* **52**, 491–498 (2014)
63. M. Algrade, M. Sultan, O.M. Samir, A. Elwhab, B. Alwany, Electronic polarizability, optical basicity and interaction parameter for Nd₂O₃ doped lithium–zinc–phosphate glasses. *Appl. Phys. A* **123**(524), 1–12 (2017)
64. J.A. Duffy, A common optical basicity scale for oxide and fluoride glasses. *J. Non Cryst. Solids* **30**, 35–39 (1989)
65. V. Dimitrov, T. Komatsu, Effect of interionic interaction on the electronic polarizability, optical basicity and binding energy of simple oxides. *J. Ceram. Soc. Jpn.* **107**, 1012–1018 (1999)
66. V. Dimitrov, S. Sakka, Linear and nonlinear optical properties of simple oxides. II. *J. Appl. Phys.* **79**, 1741–1745 (1996)
67. V. Dimitrov, T. Komatsu, Classification of simple oxides: a polarizability approach. *J. Solid State Chem.* **163**, 100–112 (2002)
68. V. Dimitrov, T. Komatsu, Effect of interionic interaction on the electronic polarizability, optical basicity and binding energy of simple oxides. *J. Ceram. Soc. Jpn.* **107**, 1012–1018 (1999)
69. J. Yamashita, T. Kurosawa, The theory of the dielectric constant of ionic crystals III. *J. Phys. Soc. Jpn.* **10**, 610–633 (1955)
70. V. Dimitrov, T. Komatsu, Interionic interactions, electronic polarizability and optical basicity of oxide glasses. *J. Ceram. Soc. Jpn.* **108**, 330–338 (2000)